

OPEN ACCESS

Surface Chemistry and Degradation Processes of Dense $\text{La}_{0.6}\text{Sr}_{0.4}\text{CoO}_{3-\delta}$ Thin Film Electrodes

To cite this article: Matthäus Siebenhofer *et al* 2023 *J. Electrochem. Soc.* **170** 014501

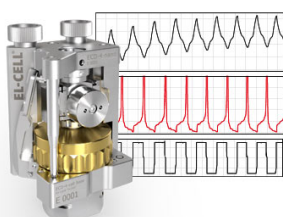
View the [article online](#) for updates and enhancements.

You may also like

- [Theoretical Study of Oxygen Vacancy Formation at LSC/GDC Interface](#)
Takayoshi Ishimoto, Kenji Sato and Michihisa Koyama
- [Improvement of Thermal Reliability and Power Density of SOFCs By Preparing Nano LSC Particles Between GDC Electrolyte and Lscf Cathode](#)
Takehito Mukai, Takahiro Fujita, Shigeki Tsukui *et al.*
- [Influence of Hetero Grain Boundaries on Oxygen Exchange Activity: Investigation of Two-Phase \$\(\text{La,Sr}\)\text{CoO}_3 / \(\text{La,Sr}\)_2\text{CoO}_{4+x}\$ Cathode Materials](#)
Sebastian Stämmler, Rotraut Merkle, Benjamin Stuhlhofer *et al.*

Measure the Electrode Expansion in the Nanometer Range.
Discover the new ECD-4-nano!


electrochemical test equipment



- Battery Test Cell for Dilatometric Analysis (Expansion of Electrodes)
- Capacitive Displacement Sensor (Range 250 μm , Resolution ≤ 5 nm)
- Detect Thickness Changes of the Individual Electrode or the Full Cell.

www.el-cell.com +49 40 79012-734 sales@el-cell.com





Surface Chemistry and Degradation Processes of Dense $\text{La}_{0.6}\text{Sr}_{0.4}\text{CoO}_{3-\delta}$ Thin Film Electrodes

Matthäus Siebenhofer,^{1,2,z} Ulrich Haselmann,³ Andreas Nennung,¹ Gernot Friedbacher,¹ Andreas Ewald Bumberger,¹ Stefan Wurster,³ Werner Artner,⁴ Herbert Hutter,¹ Zaoli Zhang,³ Jürgen Fleig,¹ and Markus Kubicek¹

¹Institute of Chemical Technologies and Analytics, TU Wien, Vienna, Austria

²Centre for Electrochemistry and Surface Technology, Wr. Neustadt, Austria

³Erich Schmid Institute of Materials Science, Leoben, Austria

⁴X-Ray Center, TU Wien, Vienna, Austria

The changes of the surface morphology and the surface chemistry of LSC thin films grown on different substrates were tracked for 100 hours under SOFC operation conditions. Atomic force microscopy was used to monitor the formation of particles at the LSC surface. Depending on the thin film structure (polycrystalline vs. epitaxial), different particle formation dynamics were observed. Electron microscopy was employed to investigate the chemistry of the segregated particles and revealed that the particles were Sr- and S-rich. Secondary ion mass spectrometry and X-ray photoelectron spectroscopy measurements were performed on degraded LSC thin films, which also found significant amounts of sulfur on the LSC surface, despite no deliberate addition of sulfur compounds, as well as A-site cation enrichment. Impedance spectroscopy was used to track the polarization resistance of LSC grown on YSZ over the same degradation period and a strong increase in the polarization resistance and in its activation energy was revealed (1.09 to 1.73 eV). The experimental results indicate that sulfur adsorption on LSC surfaces is omnipresent in the investigated conditions and even trace amounts of sulfur compounds present in nominally pure measurement gases account for particle formation and multiple degradation effects under operating conditions.

© 2023 The Author(s). Published on behalf of The Electrochemical Society by IOP Publishing Limited. This is an open access article distributed under the terms of the Creative Commons Attribution 4.0 License (CC BY, <http://creativecommons.org/licenses/by/4.0/>), which permits unrestricted reuse of the work in any medium, provided the original work is properly cited. [DOI: 10.1149/1945-7111/acada8]



Manuscript submitted August 10, 2022; revised manuscript received November 10, 2022. Published January 6, 2023.

Supplementary material for this article is available [online](#)

Perovskite-type oxides with mixed electronic and ionic conductivity are in the spotlight of research as cathode materials for solid oxide fuel cells (SOFCs).^{1,2} Since the oxygen reduction reaction on the surface of the cathode is often the rate limiting step in the operation of the fuel cell,^{3,4} optimization of materials regarding their surface properties is heavily pursued.^{5,6} Because of its high catalytic activity for this oxygen reduction reaction, $\text{La}_{0.6}\text{Sr}_{0.4}\text{CoO}_3$ (LSC) is an interesting candidate for intermediate temperature SOFCs (400 °C–600 °C).^{7,8} Despite its high surface activity, LSC suffers from significant performance degradation under operating conditions, which is commonly related to strontium segregating to the surface and blocking the oxygen exchange.^{9–11} As causes of this segregation, several factors have been identified, ranging from poisons such as SO_2 or Si and Cr sources, to elastic inequilibrium driving the strontium out of the bulk and electrostatic effects originating in surface-near regions.^{9,10,12–18} While the surface reaction already seems to be inhibited by a low amount of strontium accumulating on the surface, segregation of additional strontium is known to form particles on the perovskite surface.^{19–22} Deeper understanding of the effects of surface Sr on the oxygen exchange kinetics, segregation processes and nature and evolution of said particles is integral to develop strategies for mitigating performance degradation of SOFC cathode materials.

In this study, the evolution of LSC surfaces is traced during annealing in synthetic air at 600 °C for 100 h by atomic force microscopy (AFM) and electrochemical impedance spectroscopy (EIS). For this purpose, dense LSC thin films were grown on different substrates with pulsed laser deposition (PLD) to investigate the influence of lattice strain on the segregation process. The composition of segregated particles was analyzed using scanning electron microscopy (SEM). Furthermore, the surface chemistry of the degraded thin films was examined by means of angle resolved X-ray photoelectron spectroscopy (XPS) and time of flight secondary

ion mass spectrometry (TOF-SIMS). This contribution reports the results of these experiments and further clarifies the segregation and degradation mechanisms with regard to the surface chemistry of perovskite SOFC cathode materials.

Methods

Sample preparation.—Yttria stabilized zirconia (YSZ, 9.5 mol% Y_2O_3), SrTiO_3 (STO), LaAlO_3 and $(\text{LaAlO}_3)_{0.3}(\text{Sr}_2\text{AlTaO}_6)_{0.7}$ (LSAT) single crystals were used as substrates in this study (all $10 \times 10 \times 0.5 \text{ mm}^3$, Crystec GmbH (Germany)). Before deposition, the substrates were exposed to a thorough cleaning and annealing routine, which is described in detail in S.1. of the supporting information.

Dense $\text{La}_{0.6}\text{Sr}_{0.4}\text{CoO}_{3-\delta}$ (LSC) thin films were deposited on the single crystal substrates using PLD. All depositions were performed with a KrF excimer laser ($\lambda = 248 \text{ nm}$, Lambda Physics, COMPex Pro 201) at a laser fluence of 1.1 J cm^{-2} . 2000 laser pulses were shot at a frequency of 2 Hz and a target-substrate distance of 6.0 cm. The deposition atmosphere was set to 0.04 mbar $p(\text{O}_2)$ and the substrate was heated to a temperature of 600 °C, measured through a pyrometer (Heitronics). After deposition, the sample was cooled to room temperature at a cooling rate of 12 °C min^{-1} . For the determination of the LSC growth rate, a separate sample with 20 ZrO_2 slurry dots on the surface was prepared, which were removed after deposition. The depth of these holes was measured with a profilometer (DekTakXT, Bruker, USA) and the resulting growth rate of LSC amounted to $0.028 \pm 0.0018 \text{ nm per pulse}$.

All samples were scratched with a diamond tip for an easier locating of the (undisturbed) areas to be measured by AFM. One AFM series was measured before any annealing step to find suitable and retrievable areas. The corresponding optical microscope image was recorded to ensure reproducible alignment of the AFM tip.

Sample characterization.—Samples with thin films were examined by different X-ray diffraction (XRD) techniques. All measurements were performed in an Empyrean X-Ray diffractometer

equipped with a GaliPIX3D detector (both Malvern Panalytical Ltd.), except for grazing incidence measurements, where a PIXcel3D detector was used (Malvern Panalytical Ltd.). θ - 2θ scans were performed on all samples. A grazing incidence scan was performed on LSC deposited on YSZ, as it cannot grow epitaxially due to the severe lattice mismatch. On all other LSC thin films, reciprocal space maps of the (103) reflex were recorded in addition to θ - 2θ scans. Here the full size of the semiconductor detector was used in static area mode and ω was varied from 16 to 24°. Measurement times amounted to 60 min for each measurement. The grazing incidence diffractogram was analyzed with Panalytical Highscore.²³

Atomic force microscopy (AFM) was performed in tapping mode in a Nanoscope V multimode setup (Bruker). AFM images were analysed with the visualization software Gwyddion (Czech Metrology Institute).

Analytical scanning electron microscopy (SEM) on the surface segregates was conducted using a Leo-1525 field emission scanning electron microscope (Zeiss, Germany) equipped with a Schottky emitter and an Everhart-Thornley detector for the secondary electron (SE) images and an energy dispersive X-ray (EDX) detector (Bruker, USA). For the acceleration, a voltage of 4 kV was chosen to be as surface sensitive as possible, while still being able to detect the characteristic X-ray emission of the contained elements. Using an aperture size of 120 μm and the high current mode resulted in receiving a high signal to noise ratio while still maintaining a reasonable resolution. Monte-Carlo electron path simulations were done with Casino 2.481-3 using the trajectories of 10^4 electrons.

Secondary Ion Mass Spectroscopy (SIMS) measurements were performed on a ToF-SIMS 5 instrument (ION-TOF GmbH) in CBA-mode or CBA-burst mode^{24,25} allowing high lateral resolution and sufficient mass resolution to separate $^{32}\text{S}^-$ from $^{16}\text{O}_2^-$, simultaneously. For the investigation of secondary ions, 25 kV Bi^+ primary ions were used, for depth profiling either 1 kV Cs^+ ions or 1 kV O_2^+ ions were used for the measurement of negative and positive secondary ions, respectively. In sputter craters of an area of $300 \times 300 \mu\text{m}^2$, areas of $100 \times 100 \mu\text{m}^2$ were examined with regard to secondary ion mass and intensities, applying a 512×512 measurement raster. A low energy electron gun (21 V) was used for charge compensation.

XPS measurements were carried out at room temperature in a UHV chamber by SPECS, Germany, using a monochromated Al K-alpha source (XRC-125 MF, SPECS) operated at 80 W, and an angle resolved photoelectron analyzer (SPECS PHOIBOS WAL), collecting photoelectrons at emission angles from 20–80 degrees from the surface normal. Survey spectra were recorded at 100 eV analyzer pass energy, and detailed spectra for peak fitting were recorded at 50 eV pass energy.

Directly before insertion into the chamber, the samples were mounted on the XPS sample holder and heated up to 400 °C in air for 5 min, in order to minimize the amount of surface carbon. At this temperature and timescale, the surface cation stoichiometry is not altered.²⁶

In order to minimize quantification errors due to different photoelectron energies of the different XPS peaks, chemical quantification was focused on Sr3d, La4d, S2p, Pt4f and Co3p photoelectrons, which lie between 1330 and 1420 eV photoelectron energy. The photoelectron inelastic mean free path of these is about 2 nm.²⁷ Peak fitting and quantification were carried out with

CasaXPS software, using S-shaped "Shirley" background functions, and compositional analysis was based on the peak areas and Scofield cross Sections.²⁸ Mixed Gaussian-Lorentzian peak shapes were used for fitting the different chemical components. The Sr3d_{3/2} and Sr3d_{5/2} multiplet peaks were constrained to an energy difference of 1.7 eV, an area ratio of 2:3, and equal FWHM.

Results

Sample characterization.—Before any films were deposited on the single crystals, the surfaces of the substrates were examined by atomic force microscopy. Overview scans of $1 \mu\text{m}^2$ areas and linear scans depicting terrace steps are shown in S.2 of the supporting information. On all four different substrates, atomic terraces could be observed. After the LSC thin films were deposited on the substrates, XRD measurements were performed on all samples to analyze the strain state of the thin films, a summary is shown in Table I and detailed results are shown in Fig. 1. Reciprocal space maps (RSMs) showed that the in-plane lattice parameter of the substrate was imposed on the thin film for STO, LAO and LSAT, clearly visible as the reflexes of substrate and film are aligned with regard to q_x . The out-of-plane lattice parameter varies conversely to the in-plane strain.

AFM scans of all thin films showed that their surface always exhibits a certain mosaicity (Fig. 1). In combination with XRD and TEM measurements, the experiments revealed a columnar polycrystalline growth of LSC on YSZ and epitaxial growth (most probably with small-angle grain boundaries) on the other substrates. The RMS roughness values of the pristine thin films are also depicted in Table I, showing that of all LSC thin films, those grown on YSZ exhibited the roughest surface, followed by STO, LSAT and LAO. On pristine LSC thin films grown on STO, several uniformly distributed cracks were found during AFM measurements (Fig. 1), probably as a consequence of the strong tensile strain imposed by the STO substrate.

Surface morphology of LSC thin films.—To trace the evolution of the LSC surface morphology during degradation, a $10 \times 10 \mu\text{m}^2$ area adjacent to the diamond tip marks was investigated. It is noteworthy that on pristine samples, no particles could be observed. Therefore, any Sr segregation occurring during deposition or during cooling after the deposition seems to take place on sub-nm level without particle formation. This does, however, not exclude the formation of an SrO termination layer (as was found by several authors in past studies).^{26,29-31}

To investigate particle formation processes, AFM measurements were performed after different annealing steps in synthetic air. First, all samples were heated to 450 °C ($15 \text{ }^\circ\text{C min}^{-1}$) and cooled immediately upon reaching that temperature ($15 \text{ }^\circ\text{C min}^{-1}$). AFM studies of these samples showed that the only sample undergoing noticeable changes was the STO sample, where many small, round particles were found, indicating that particle formation (Sr-rich, see below) on the LSC/STO system starts at surprisingly low temperatures. This is especially interesting with regard to the strain state of LSC on STO, which exhibits the strongest tensile in-plane strain. This is in accordance with literature reports which also find that tensile strain facilitates cation segregation.^{32,33} The LSC surface on all other substrates was not affected by this first heating step.

Table I. In-plane (i.p.) and out-of-plane (o.p.) lattice parameters of all substrates and thin films as well as RMS roughness values for pristine thin films.

Substrate	Substrate i.p. (Å)	LSC i.p. (Å)	LSC o.p. (Å)	RMS roughness (nm)
YSZ	5.12	3.82	3.82	0.244
STO	3.90	3.90	3.78	0.222
LAO	3.80	3.80	3.92	0.124
LSAT	3.86	3.86	3.81	0.146

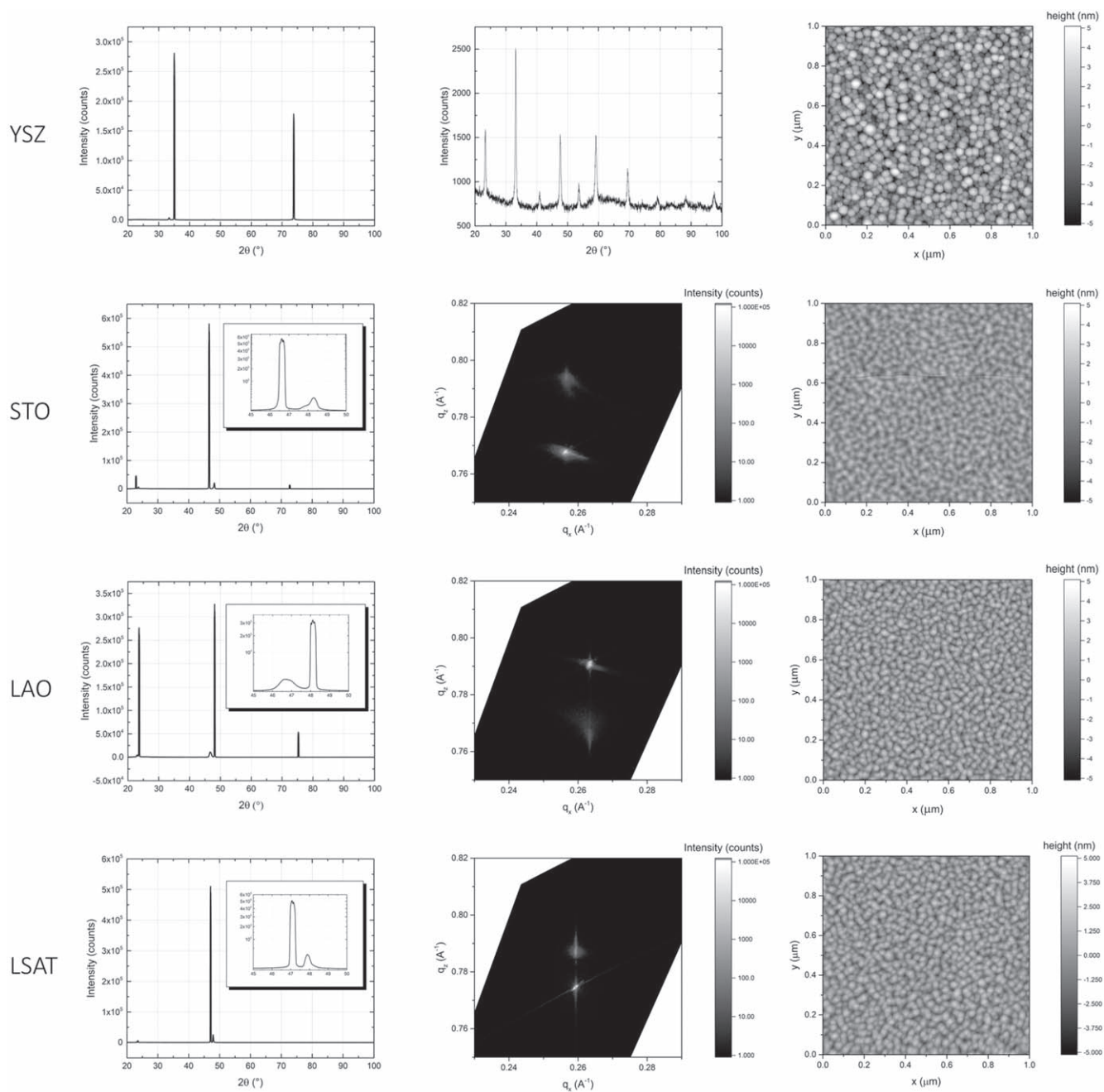


Figure 1. θ - 2θ , GID and AFM measurements of LSC on YSZ; θ - 2θ , RSM and AFM measurements of LSC on STO, LAO and LSAT.

Next, the samples were heated to 600 °C and cooled immediately afterwards. As a result, particles were observed on all surfaces (not shown here). Again, the highest particle density was present on STO, followed by YSZ, LSAT and LAO. Interestingly, on STO the particle density decreased significantly when approaching a surface crack. With regard to the morphology of the segregates, there are no significant differences between the specific substrates at this point, all segregates are round (~ 20 – 30 nm diameter) and of similar height (~ 5 – 10 nm).

First significant differences appear after 3 h annealing time at 600 °C (see Fig. 2, lhs). While the number of segregates increases on all substrates, their shape becomes qualitatively different depending on the substrate. Segregates on YSZ and STO retain a smaller size, on LAO and LSAT, however, large and flat segregates with a smooth surface emerge from the LSC film. The shape of these segregates indicates a single crystalline structure of the particles and

similar particles have been previously observed on the surface of polycrystalline LSC.^{22,34} This trend of particle formation on LAO and LSAT continues for the next 30 h (see Fig. 2, rhs). The large and flat segregates continue to grow in size and small particles appear in between. Based on the size of these particles, we can conclude that substantial amounts of material have to migrate to the surface and leave behind a significantly altered host material.

LSC grown on YSZ exhibits different segregation dynamics. On YSZ, the lowest coverage of the LSC surface with particles is observed. The shape of the particles is pointed and only after very long annealing times (>30 h), large segregates can be observed. On STO, it further appears as if the initially present cracks heal with increasing annealing time and more and more particles grow on the surface. However, after 10 h, AFM images show that particles start to form inside the cracks and that the cracks are filled with material. This trend continues and very large particles appear on top of the

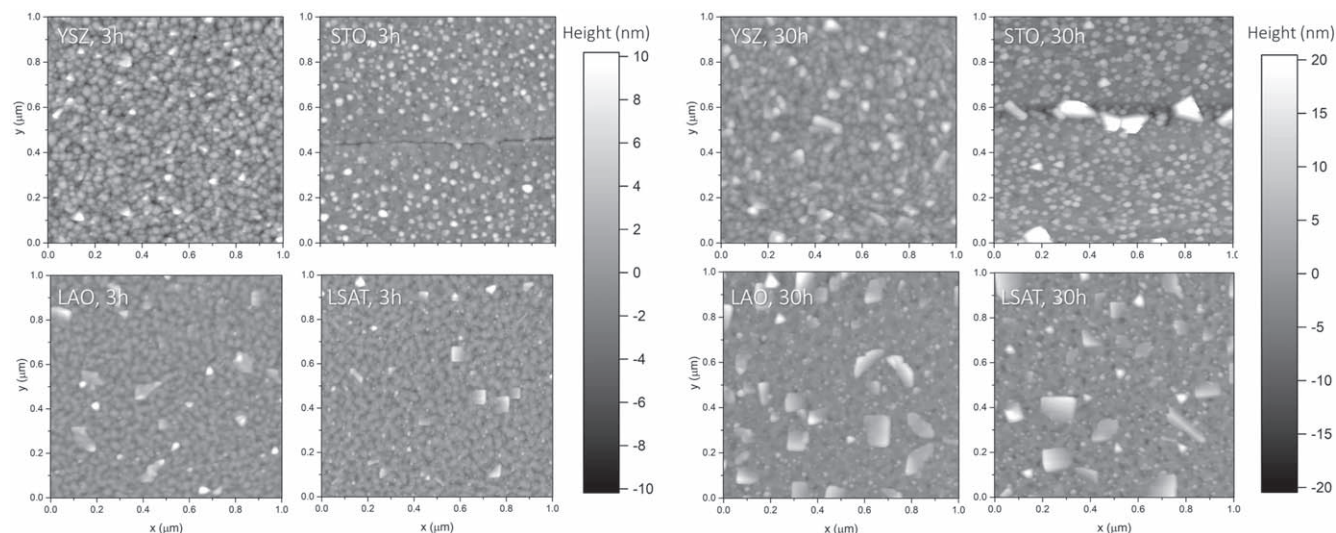


Figure 2. LSC surfaces on different substrates after annealing in synthetic air at 600 °C for 3 h and 30 h.

cracks. Possibly, due to the strain-relaxed state around the cracks, segregation to the surface is not preferable and material rather migrates laterally toward the cracks, which are continuously filled with increasing annealing time. After 100 h annealing in synthetic air, the so far observed trends continue, particles grow larger and more particles appear. Furthermore, from 30 h onwards, depressions on the surface of films grown on perovskite substrates appear, possibly indicating that large amounts of material migrate and participate in particle formation processes on the surface. The complete evolution of the surface of LSC thin films grown on different substrates is shown in Fig. 3.

The AFM images were further analyzed with regard to particle properties, surface coverage and surface roughness (Fig. 4). The mean diameter of the segregated particles increases from around 10 nm to up to 20 nm depending on the substrate. This is, however, a superposition of two effects, as the mean particle diameter is heavily influenced by newly formed smaller particles. The maximum particle diameter can surpass 100 nm for the biggest segregates. The analysis further shows that the surface coverage of segregated particles continuously increases to around 25%–30% after 100 h on perovskite substrates and to 16% on YSZ. Further, the surface roughness continuously increases over the whole 100 h period.

Surface chemistry of LSC thin films.—SIMS measurements were performed on the same LSC thin films which were investigated by AFM, grown on all four different substrates and annealed for 100 h in synthetic air, to assess the depth distribution of different cations in the thin film and to check for impurities on the surface or in the film. While these measurements allow an assessment of the total surface chemistry, it is not possible to distinguish between segregated particles and free LSC surface, the results are always a representation of the average surface chemistry. In Fig. 5, positive secondary ion intensities of the cations Co, Sr, and La are plotted normalized to their respective bulk values. As the intensity of ^{88}Sr was already close to the saturation limit, the isotope ^{86}Sr is also plotted for reference (see differences in STO and LSAT). At the surface and interface regions, certain deviations from the bulk values are expected due to changes in surface conductivity and ionization probability for different ions. While those changes are difficult to interpret, qualitative changes between samples are, however, more straightforward to understand. In that regard, most notably, a strong Sr enrichment was found for LSC|YSZ and to a lesser extent in LSC|LAO and LSC|LSAT as well as in LSC|STO with the weakest increase. Similarly, La seems to accumulate on the outermost surface (especially for LSC grown on STO), however, there also appears to be a slight La depletion zone directly below the surface. Moreover,

for all LSC thin films grown on perovskite substrates, a Co enrichment in surface regions was found. Furthermore, SIMS measurements revealed significant amounts of sulfur on top of all samples (Fig. 5), indicating that traces of sulfur compounds (which are present in all measurement gases, e.g. ~ 0.5 ppmv in 5.0 purity O_2 , fed through a standard pressure reducer and tubing,^{35,36}) accumulate on the LSC surface during annealing. The near-surface decrease observed in the oxygen signal is attributed to the overlap with the sulfur signal, as can be seen in the mass spectrum.

In addition, angle resolved XPS measurements were performed on the identical LSC thin films grown on YSZ and STO. For comparison, additional pristine thin films were deposited and each pristine sample was split into two parts, one of which was washed with bidistilled water to remove water soluble surface species formed as an equilibrium surface layer at high temperatures. At this point it is noteworthy that the kinetic effect of washing has been discussed in earlier studies,^{26,31} which found a significant improvement of the surface exchange kinetics, indicating a strong detrimental effect of the water soluble species on the surface. All six samples were investigated by XPS (see Fig. 6). Again, XPS results include contributions from all features present on the respective surfaces and do not allow to distinguish between particles and free surface. For degraded LSC grown on STO, photoelectron spectra in the La 4d region reveal an enrichment of La in the top most layer of the thin film, while this difference is not visible for LSC grown on YSZ. With regard to Sr-rich surface species, XPS spectra show two major Sr components—one surface species primarily visible on pristine LSC surfaces and only very weakly on washed surfaces, likely indicating a correlation with an equilibrium SrO termination and one species which was previously attributed to SrSO_4 .³⁵ The latter assignment is again confirmed by a strong S signal appearing on degraded thin films. Surprisingly, the SrO correlated signal intensity is less pronounced in degraded films compared to pristine films. The signal of the SrSO_4 species increases significantly on degraded films, especially for the polycrystalline LSC grown on YSZ. With regard to the surface reaction we suggest that, due to the high oxygen content of synthetic air, the predominant sulfur impurity is SO_2 which reacts with the SrO termination and, upon further oxidation, forms SrSO_4 .

The same trend can also be observed for the oxygen signal, i.e. the signal intensity of the SO_4^{2-} -related oxygen species is strongly increased in degraded films. This oxygen species has been related to SO_4^{2-} by detailed XPS measurements in a previous study.³⁵ An SO_4^{2-} -related oxygen species is also indicated for pristine and washed films, however, as the sulfur signals reveal, next to no

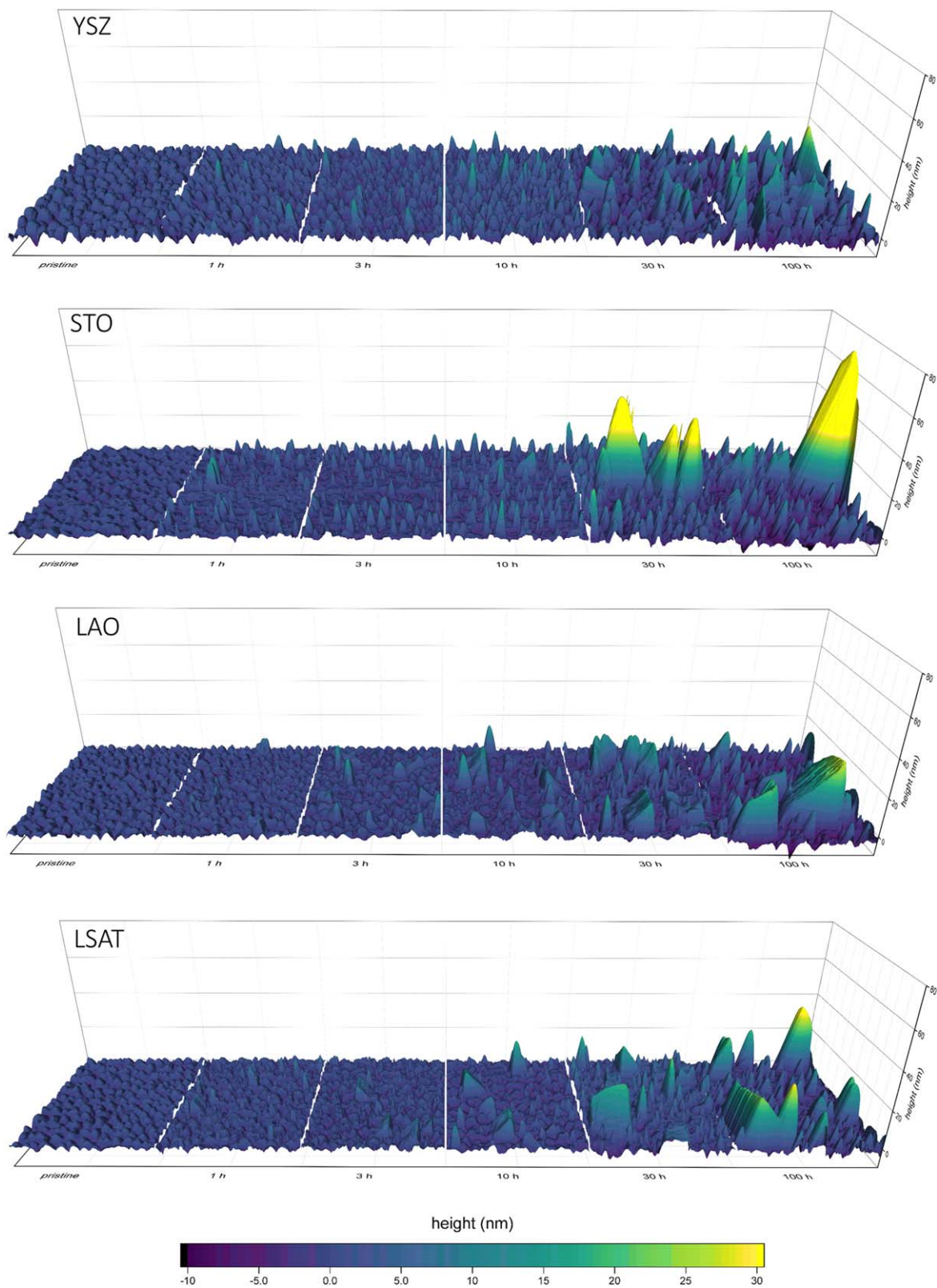


Figure 3. 3D visualization of the surface morphology of LSC thin films grown on YSZ, STO, LAO and LSAT after different annealing times at 600 °C in synthetic air. Each surface map is assembled of six $0.5 \times 0.5 \mu\text{m}^2$ AFM images recorded at specific experiment steps. Height-zero is set at the mean value of a region without large segregates.

sulfur is present on these films. Therefore, we suspect that this oxygen species is connected to other surface features (e.g. remaining carbonates on the surface, a common observation for samples which had been exposed to ambient atmosphere before XPS). We also want

to emphasize that this oxygen species is present in multiple studies of the oxygen exchange kinetics of LSC and similar materials and may easily be misinterpreted if sulfur is omitted from the discussion.³⁵ The slight shifts in the binding energy of this feature

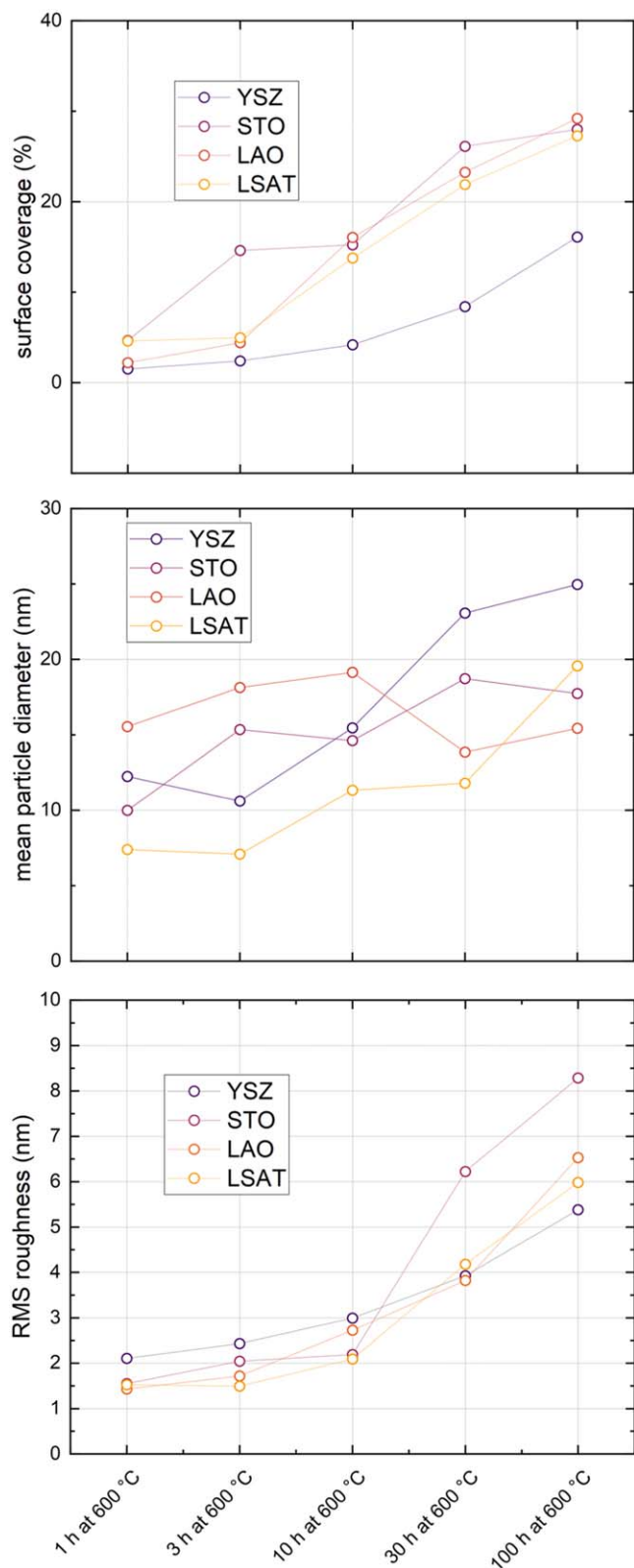


Figure 4. Analysis of LSC surfaces after different annealing times in synthetic air at 600 °C.

may correspond to the different chemical environment of carbonates and sulphates on LSC grown on YSZ and on STO. A second oxygen species was observed, though its origin is not fully clear. We suspect that it is not connected with SrO but is a feature of the metallic electronic structure of LSC. The cobalt signal (not shown) did not

yield any notable trends. Its intensity was lower for the degraded films which was expected due to particle formation and Sr enrichment on the surface. The combination of SIMS and XPS results indicate that the total surface of degraded LSC thin films contains significant amounts of sulfur compounds as well as a higher concentration of A-site cations (Sr for LSC grown on YSZ and Sr as well as La for LSC grown on STO). Purely based on these measurements it is, however, not possible to assign these effects to either particle formation or the free surface.

To specifically probe the chemical composition of the segregated particles, analytical SEM studies were conducted on an LSC thin film grown on YSZ, which was heavily degraded in ambient air at 600 °C for 100 h to facilitate the formation of big particles for a conclusive EDX analysis. Figure 7 a shows the SEM image of surface segregations of different sizes recorded with 4 keV. In the EDX elemental maps of La- $M_{\alpha\beta}$ (Fig. 7b) and Co-L (Fig. 7c) a significant reduction of the signal intensity is visible at the larger segregated particles, while seeing an increase in the Sr-L intensity (Fig. 7d), as well as in the S- K_{α} intensity at the location of the same particles. In an overlay of the three elements in Fig. 7e, it becomes obvious that the large segregated particles are indeed Sr rich and contain large amounts of sulfur. A similar phenomenon has also been observed for LSCF thin films³⁷ and sulfur signals have also been detected for similar segregates on polycrystalline LSC.^{22,34}

To investigate, why no higher Sr content could be observed for the small segregated particles in the SE-SEM image, Monte-Carlo electron path simulations were conducted using Casino 2.481–3. The simulations show that the lateral diameter of the interaction volume is larger than 200 nm in diameter, hindering the resolution of smaller features in the elemental maps. Additionally, for smaller segregates, the proportion of the EDX signal stemming from the film increases. Therefore, from EDX measurements, it is not possible to conclusively determine the exact composition of the smaller particles. However, our measurements clearly indicate that they also contain sulfur as the S map identifies more particles than the Sr map, due to the stronger contrast compared to the rest of the thin film.

In addition to SEM investigations, degraded epitaxial LSC thin films were examined with XRD. However, this analysis was inconclusive and, apart from background noise, no clear Sr-containing phases could be identified. This may be caused by a preferential orientation of the segregates or by the low amount of material available for X-ray diffraction.

Oxygen exchange kinetics of degraded LSC.—The area specific resistance of LSC was tracked with electrochemical impedance spectroscopy during 100 h of degradation in synthetic air at 600 °C. As STO, LAO and LSAT are mixed conductors or insulators, this was only possible for LSC grown on a YSZ single crystal. For this purpose, 55 nm LSC thin films were grown on both sides of a YSZ single crystal with current collecting Ti/Pt grids beneath LSC on both sides. Impedance spectra were recorded during degradation and the evolution of the area specific resistance is shown in Fig. 8. Considering the shape of the impedance curves which does not change during the degradation process, as well as the capacitive properties which agree well with a chemical capacitance, we conclude that the resistance origin lies in the oxygen exchange reaction at the surface and that it is mainly the corresponding reaction rate which is affected by the degradation process (for detailed impedance spectra see S.I.4 in the supporting information). The resistance continuously increases during the whole experiment, with the total resistance being higher than in a previous similar study but in the same order of magnitude.³⁸ Additionally, the activation energy of the surface exchange resistance was investigated before and after degradation. The results of these measurements show that the activation energy increases significantly during degradation, from 1.09 eV during the first heating in the ex situ setup up to 1.73 eV during cooling after 100 h of degradation. We also investigated the oxygen exchange kinetics with ¹⁸O tracer exchange and secondary ion mass spectrometry, however, the obtained results

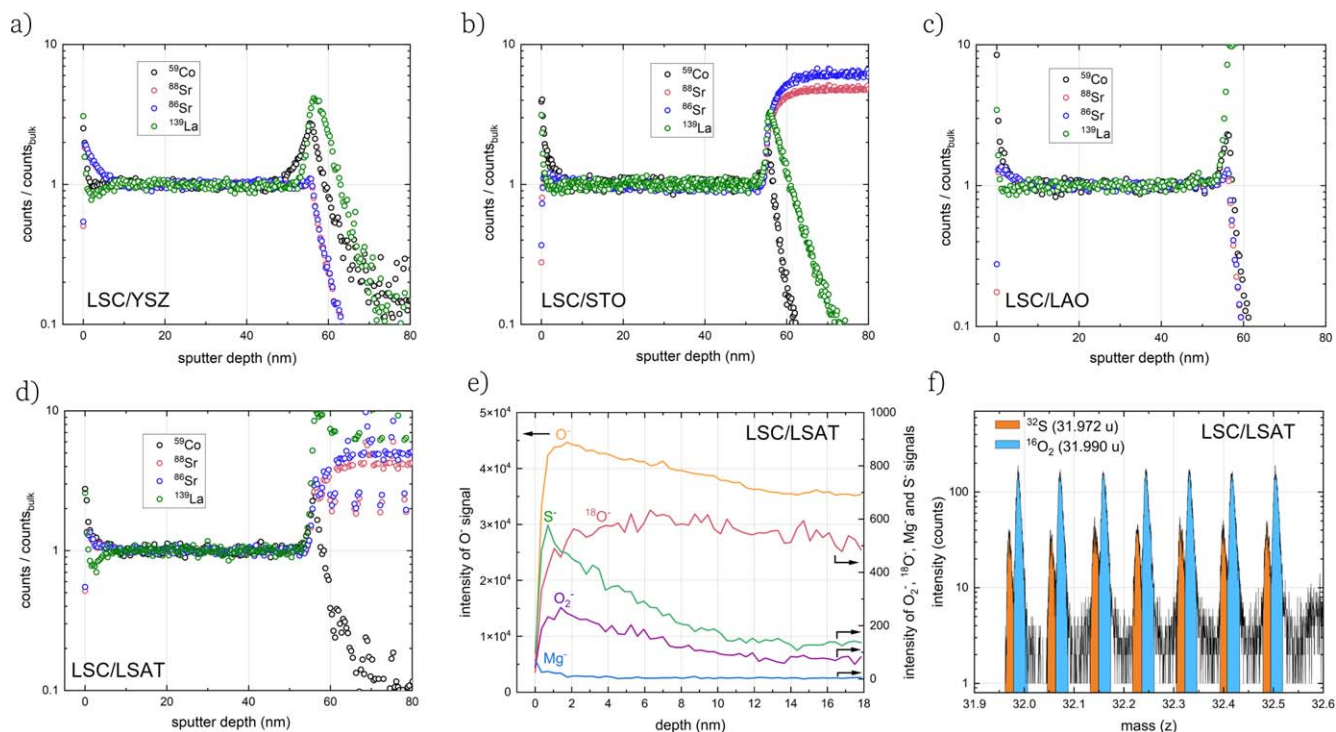


Figure 5. SIMS measurements for Co⁺, La⁺ and two Sr⁺ isotopes on 55 nm LSC thin films grown on (a) YSZ, (b) STO, (c) LAO and (d) LSAT and annealed in synthetic air for 100 h at 600 °C, normalized to bulk values. (e) depth profile for different negative ions in LSC grown on LSAT, (f) mass spectrum of S and O₂ recorded for LSC grown on LSAT in CBA-burst mode.²⁵ The mass scale is only valid for the first burst.

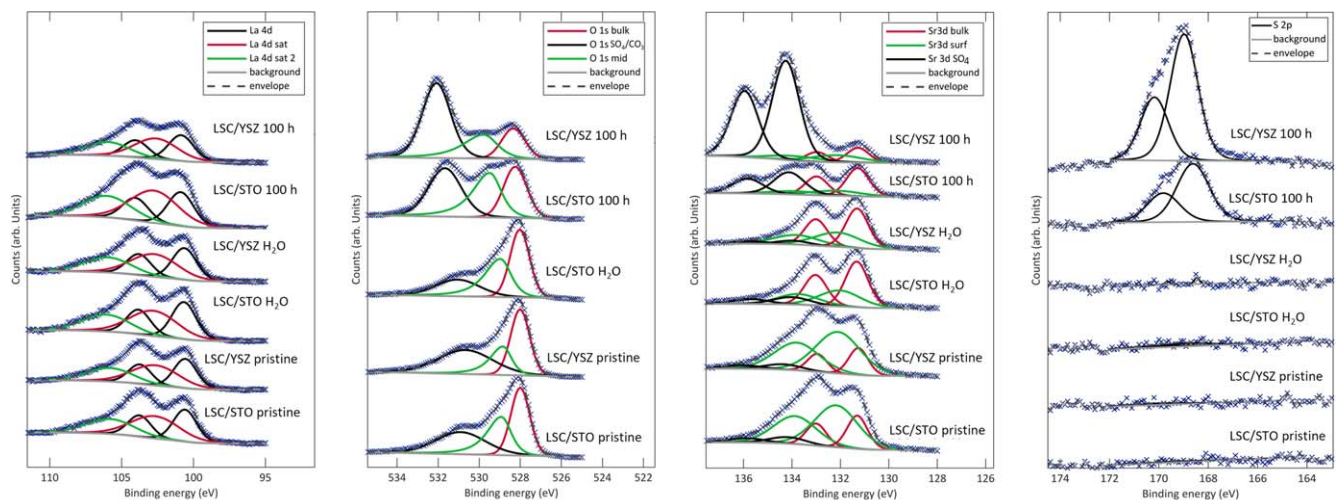


Figure 6. Photoelectron spectra of La (with all satellite peaks), O, Sr and S of different states of LSC thin films grown on YSZ and on STO. LSC YSZ/STO 100 h represents a thin film grown on YSZ/STO and annealed in synthetic air at 600 °C for 100 h. LSC YSZ/STO H₂O describes a pristine LSC thin film grown on YSZ/STO which has been washed in bidistilled water to remove water-soluble surface species. LSC YSZ/STO pristine represents a pristine LSC thin film directly after deposition.

are not straightforward to interpret and were not conclusive with regard to the effect of surface Sr and secondary phases. Potentially, tracer exchange in combination with SIMS is not a suitable method to assess the oxygen exchange kinetics of heavily degraded LSC thin films (see S.3 in the supporting information).

Discussion

The combination of the measurements presented here clarifies that a major part of the particles found on top of degraded LSC thin films contain large amounts of sulfur, most likely forming sulfate compounds with LSC cations. SIMS and XPS results suggest, that

while for polycrystalline LSC grown on YSZ, basically all particles consist of SrSO₄, especially for epitaxial LSC grown on STO, also other sulfate species like La₂(SO₄)₃ could constitute a part of the observed segregates. It is also clear that the accumulation of sulfur at the LSC surface is inseparably linked to cation segregation to the surface and to the performance degradation of SOFC cathodes. Most presented experiments were performed in synthetic air, which is nominally sulfur free. Our study therefore also confirms earlier results^{36,39} that measurements with nominally clean bottled gases may easily lead to trace amounts of sulfur in the measurement setup (~0.5 ppmv using 5.0 purity O₂, measured with ICP-MS³⁵), which

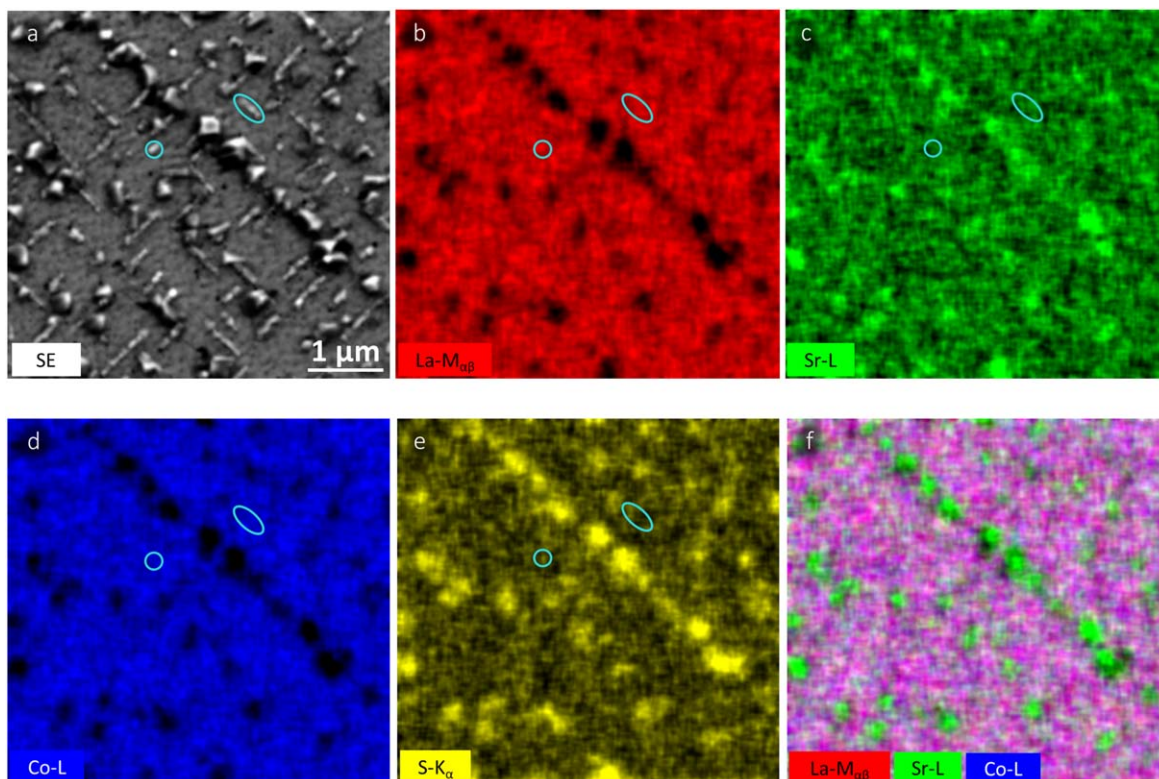


Figure 7. SEM EDX images of an LSC thin film grown on YSZ and continuously annealed for 100 h in ambient air at 600 °C.

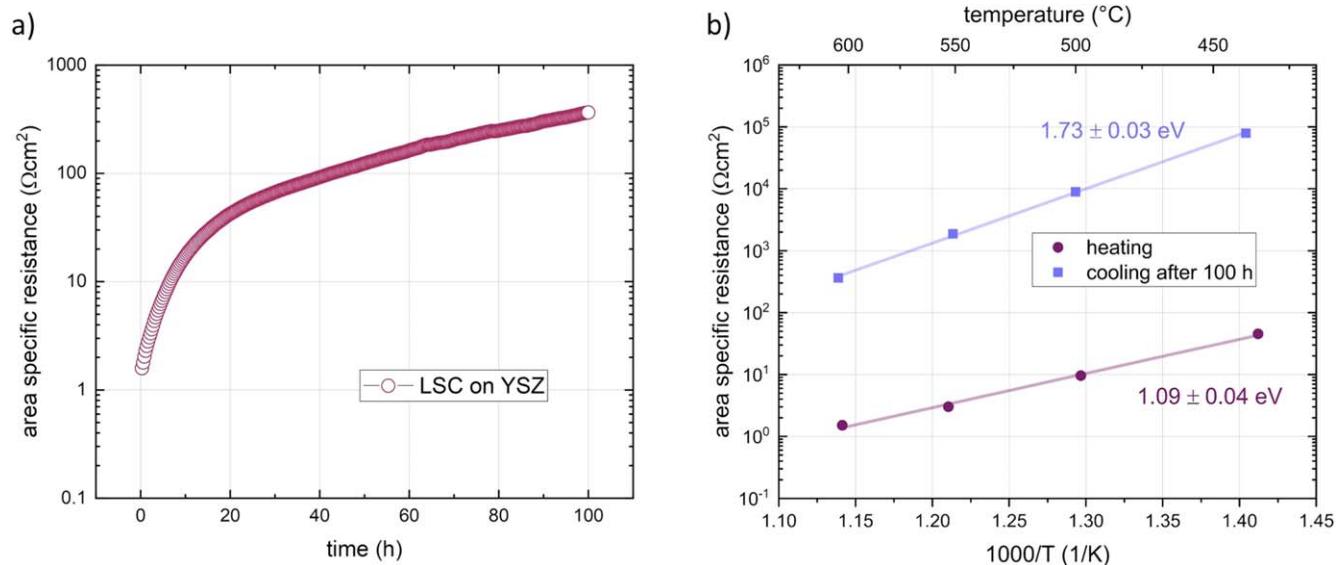


Figure 8. a) Evolution of the area specific resistance of 55 nm LSC grown symmetrically on a YSZ single crystal during degradation in synthetic air at 600 °C for 100 h. b) Temperature dependence of the area specific resistance of 55 nm LSC grown symmetrically on a YSZ single crystal before and after degradation.

are very relevant for the poisoning of cathode surfaces in measurement environments.

With regard to the dynamics of particle formation and segregation, the experiments show that the thin film microstructure is critical for the type and extent of segregation, possibly even more than lattice strain. Epitaxial thin films tend to produce a combination of large, flat segregates and smaller ball-like particles, while on polycrystalline thin films, medium sized pointed segregates are observed. We strongly suspect that this behavior is related to grain boundaries acting not only as a pathway for segregating material, but also as preferable segregate location.^{29,32,40}

The discussion of the correlation between cation segregation and the oxygen exchange kinetics of LSC is less straightforward. In literature, Sr segregation is commonly described to be a main reason for the performance degradation of LSC.^{17,30} Among the variety of discussed phenomena are, for example, an SrO top layer with a detrimental effect on surface exchange kinetics,²⁶ La and Sr containing oxide phases which cover electrochemically active sites²¹ and leave behind a chemically altered host material⁴¹ as well as heterogeneously distributed SrO/Sr(OH)₂ phases.³⁰ Additionally, sulfur poisoning effects were described in detail and trace amounts of sulfur were already found to affect the surface

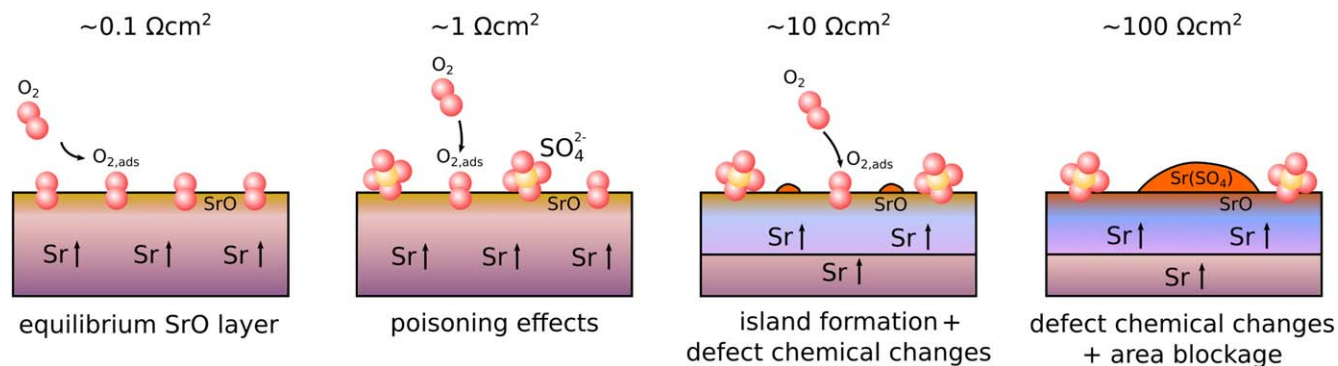


Figure 9. Overview of different degradation phenomena observed on LSC thin films during annealing in synthetic air at 600 °C with estimated values for the oxygen exchange resistance, SrO indicates the termination layer.

exchange kinetics of polycrystalline LSC in long term experiments.^{10,39,42} Recent in situ PLD studies have further shown that the very high catalytic activity of pristine LSC thin films immediately decreases when the sample is transferred to an ex situ setup,^{18,36} caused by the adsorption of trace amounts of sulfur on the entire LSC surface, leading to a strong and very fast degradation.³⁵

Based on the substantial amount of literature on the degradation behavior of LSC and the results of this study, we suggest the following model for the evolution of the oxygen exchange kinetics of dense LSC thin films (Fig. 9): (1) Sr segregation occurs in all thin films and leads to an equilibrium (at least partial) SrO termination of the perovskite surface surface, which still contains surface vacancies for oxygen exchange^{26,30,31} and is not considered to be a separate second phase. In this state, the oxygen exchange kinetics can be very fast and, in accordance with recent results by Nicolle et al., the SrO termination could even be beneficial for oxygen exchange kinetics.^{18,43–45} (2) Sulphur contaminations in the atmosphere adsorb on the surface and form SO_4^{2-} adsorbates which strongly inhibit the oxygen exchange on the LSC surface by a yet unknown mechanism (fast initial degradation).^{18,35} (3) Continuing sulfur adsorption in combination with Sr segregation leads to the formation of secondary phases and small particles⁵⁰, preferably located in and on top of grain boundaries and microcracks, whose growth is facilitated by tensile lattice strain. These particles leave behind a substantially altered host material with modified A/B cation ratios, having a further detrimental effect on the oxygen exchange kinetics (long term degradation and activation energy change). (4) Large Sr-rich particles form on the LSC surface and block available surface area, with epitaxial surfaces promoting the growth of very large and flat segregates.

All individual steps of this degradation model have already been presented individually in literature. Here, we bring them together by suggesting a sequence of degradation steps modifying the perovskite surface. The first two steps in the evolution of the LSC surface chemistry have already been discussed in Refs. 26, 30, 31, 35, 46. However, literature studies often neglect the effect of acidic adsorbates like sulfur in their discussion of the kinetic effect of an SrO termination layer. According to recent studies, basic oxides (like SrO) enhance the oxygen exchange kinetics of mixed conducting oxide surfaces.^{43,47} Thus, we suspect that many of the negative effects that have been attributed to an SrO termination are in fact caused by acidic adsorbates which likely react with SrO. In accordance with other reports,^{10,39,50} the present study additionally emphasizes the very important role of sulfur also in the subsequent evolution of the oxygen exchange kinetics over time. The continuous formation of S-rich particles shows that the sulfur amount on the LSC surface steadily increases with time. Equally, the polarization resistance also increases continuously over 100 h. However, the pure blockage of parts of the surface by particles can neither explain the observed degradation over 2 orders of magnitude, nor the changed

activation energy. Rather, the remaining particle-free surface has to change drastically over time.

As a consequence of the S and Sr-rich secondary phase formation, we suggest that the host material undergoes a significant alteration of its chemical composition and thus also exhibits a strongly different near-surface defect chemistry,⁴⁶ which causes the considerable increase of the activation energy after annealing (step 3 and step 4). Surface analytical measurements argue against a growing continuous surface layer (e.g. SrO), as all cations are still present in significant concentrations in near-surface regions after annealing. A likely explanation for this continuous effect on the oxygen exchange kinetics and its activation energy is a gradual change of the surface defect chemical equilibrium constants, e.g. by a change of the oxygen vacancy formation enthalpy, caused by the altered host material composition.^{48,49} Finally, also the total amount of available free surface is affected by degradation processes, as particles grow and consume considerable parts of the LSC surface (up to 30% in the present experiments), although we suggest that this only causes a minor part of the entire resistance increase (step 4).

These considerations strongly suggest the conclusion that surface Sr does not necessarily have a detrimental effect on the surface exchange kinetics of LSC, but when being accompanied by the adsorption of sulfur and the formation of SO_4^{2-} -adsorbates and secondary phases, which (directly or indirectly) cause a strong performance degradation. We suspect that the same holds in the presence of other acidic contaminants like CO_2 , CrO_3 or SiO_2 ,^{43,50} which might lead to a similar sequence of degradation steps as shown in this study and affect the oxygen exchange kinetics of LSC and other SOFC cathode materials in similar ways.

Conclusions




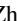


The surface morphology and surface chemistry of LSC thin films grown on different substrates were investigated upon degradation in synthetic air at 600 °C. Atomic force microscopy was used to trace the evolution of the LSC surface and potential particle formation over the course of 100 h. The study reveals that particle formation already starts at low temperatures (~450 °C) and follows different dynamics, depending on the thin film structure. On polycrystalline LSC grown on YSZ, small particles form, potentially assisted by Sr diffusion via grain boundaries. In epitaxial thin films grown on perovskite substrates, beginning segregation is strain dependent, while during later stages, large and flat particles develop on the LSC surface. Scanning electron microscopy was used to investigate the chemistry of segregated particles and large segregates were found to be Sr and S rich. SIMS and XPS measurements also identified large amounts of sulfur on the surface and an A-site cation enrichment in the upmost thin film region (particles and free surface), further supporting the formation of sulfate phases on the LSC surface due to trace amounts of sulfur in all measurement gases.

The oxygen exchange kinetics of degraded thin films was investigated with electrochemical impedance spectroscopy which revealed a steady increase of the polarization resistance over time, as well as a substantial increase of the activation energy during degradation. The presented results strongly suggest that performance degradation of dense LSC surfaces is not tied to area blockage by sulfate particle formation but to changes of the surface chemistry itself. In combination with recent findings on the degradation behavior of LSC and the kinetic capabilities in its pristine state, it seems likely that the presence of Sr alone at the LSC surface itself is not responsible for the observed performance decrease under operation conditions. Strong Sr segregation is rather always accompanied or even driven e.g. by sulfur adsorption on the surface which causes an initial and immediate degradation step, followed by the formation of sulfate phases which strongly alter the chemistry of the host material. Later on, segregates conglomerate and form large particles on the thin film surface. The results of this work emphasize that, possibly even more so than on the suppression of Sr segregation, research should be focused on the development of cathode materials with a high stability toward sulfate formation to ensure fast oxygen exchange kinetics and maximal long-time operability.

Acknowledgments

The authors like to acknowledge the financial support and open access funding provided by the Austrian Science Fund (FWF) project P31654-N37. M.S. was also partly supported by the Competence Center for Electrochemical Surface Technology (CEST) in the framework of the COMET scheme of the Austrian Research Promotion Agency (FFG, project 865864).

ORCID

Matthäus Siebenhofer  <https://orcid.org/0000-0002-6450-0261>
 Andreas Nennung  <https://orcid.org/0000-0001-9313-3731>
 Andreas Ewald Bumberger  <https://orcid.org/0000-0001-9346-4864>
 Zaoli Zhang  <https://orcid.org/0000-0002-7717-2500>
 Jürgen Fleig  <https://orcid.org/0000-0002-8401-6717>
 Markus Kubicek  <https://orcid.org/0000-0001-6623-9805>

References

1. A. Jun, J. Kim, J. Shin, and G. Kim, "Perovskite as a cathode material: a review of its role in solid-oxide fuel cell technology." *ChemElectroChem*, **3**, 511 (2016).
2. S. K. Burnwal, S. Bharadwaj, and P. Kistaiah, "Review on MIEC cathode materials for solid oxide fuel cells." *J. Mol. Eng. Mater.*, **4**, 1630001 (2016).
3. S. B. Adler, "Factors governing oxygen reduction in solid oxide fuel cell cathodes." *Chem. Rev.*, **104**, 4791 (2004).
4. H. J. Bouwmeester, H. Kruidhof, and A. Burggraaf, "Importance of the surface exchange kinetics as rate limiting step in oxygen permeation through mixed-conducting oxides." *Solid State Ionics*, **72**, 185 (1994).
5. H. J. Choi et al., "Surface tuning of solid oxide fuel cell cathode by atomic layer deposition." *Adv. Energy Mater.*, **8**, 1802506 (2018).
6. D. Ding, X. Li, S. Y. Lai, K. Gerdes, and M. Liu, "Enhancing SOFC cathode performance by surface modification through infiltration." *Energy Environ. Sci.*, **7**, 552 (2014).
7. J. Hayd, L. Dieterle, U. Guntow, D. Gerthsen, and E. Ivers-Tiffée, "Nanoscaled $\text{La}_{0.6}\text{Sr}_{0.4}\text{CoO}_{3-\delta}$ as intermediate temperature solid oxide fuel cell cathode: microstructure and electrochemical performance." *J. Power Sources*, **196**, 7263 (2011).
8. L. Dieterle, P. Bockstaller, D. Gerthsen, J. Hayd, E. Ivers-Tiffée, and U. Guntow, "Microstructure of nanoscaled $\text{La}_{0.6}\text{Sr}_{0.4}\text{CoO}_{3-\delta}$ cathodes for intermediate-temperature solid oxide fuel cells." *Adv. Energy Mater.*, **1**, 249 (2011).
9. E. Bucher, M. Yang, and W. Sitte, "In situ investigations of the chromium-induced degradation of the oxygen surface exchange kinetics of IT-SOFC cathode materials $\text{La}_{0.6}\text{Sr}_{0.4}\text{CoO}_{3-\delta}$ and $\text{La}_{0.58}\text{Sr}_{0.4}\text{Co}_{0.2}\text{Fe}_{0.8}\text{O}_{3-\delta}$." *J. Electrochem. Soc.*, **159**, B592 (2012).
10. E. Bucher, C. Gspan, and W. Sitte, "Degradation and regeneration of the SOFC cathode material $\text{La}_{0.6}\text{Sr}_{0.4}\text{CoO}_{3-\delta}$ in SO_2 -containing atmospheres." *Solid State Ionics*, **272**, 112 (2015).
11. P. Hjalmarsson, M. Sjøgaard, and M. Mogensen, "Electrochemical performance and degradation of $(\text{La}_{0.6}\text{Sr}_{0.4})_{0.99}\text{CoO}_{3-\delta}$ as porous SOFC-cathode." *Solid State Ionics*, **179**, 1422 (2008).
12. E. Bucher, C. Gspan, F. Hofer, and W. Sitte, "Post-test analysis of silicon poisoning and phase decomposition in the SOFC cathode material $\text{La}_{0.58}\text{Sr}_{0.4}\text{Co}_{0.2}\text{Fe}_{0.8}\text{O}_{3-\delta}$ by transmission electron microscopy." *Solid State Ionics*, **230**, 7 (2013).
13. Z. Yang, M. Guo, N. Wang, C. Ma, J. Wang, and M. Han, "A short review of cathode poisoning and corrosion in solid oxide fuel cell." *Int. J. Hydrogen Energy*, **42**, 24948 (2017).
14. H. Ding, A. V. Virkar, M. Liu, and F. Liu, "Suppression of Sr surface segregation in $\text{La}_{1-x}\text{Sr}_x\text{Co}_{1-y}\text{Fe}_y\text{O}_{3-\delta}$: a first principles study." *Phys. Chem. Chem. Phys.*, **15**, 489 (2013).
15. H. Kwon, W. Lee, and J. W. Han, "Suppressing cation segregation on lanthanum based perovskite oxides to enhance the stability of solid oxide fuel cell cathodes." *RSC Adv.*, **6**, 69782 (2016).
16. J. Y. Koo, H. Kwon, M. Ahn, M. Choi, J.-W. Son, J. W. Han, and W. Lee, "Suppression of cation segregation in $(\text{La,Sr})\text{CoO}_{3-\delta}$ by elastic energy minimization." *ACS Appl. Mater. Interfaces*, **10**, 8057 (2018).
17. B. Koo, K. Kim, J. K. Kim, H. Kwon, J. W. Han, and W. Jung, "Sr segregation in perovskite oxides: why it happens and how it exists." *Joule*, **2**, 1476 (2018).
18. M. Siebenhofer, T. M. Huber, G. Friedbacher, W. Artner, J. Fleig, and M. Kubicek, "Oxygen exchange kinetics and nonstoichiometry of pristine $(\text{La}_{0.6}\text{Sr}_{0.4})_{0.99}\text{CoO}_{3-\delta}$ thin films unaltered by degradation." *J. Mater. Chem. A*, **8**, 7968 (2020).
19. Y. Chen, H. Tellez, M. Burriel, F. Yang, N. Tsvetkov, Z. Cai, D. W. McComb, J. A. Kilner, and B. Yildiz, "Segregated chemistry and structure on (001) and (100) surfaces of $(\text{La}_{1-x}\text{Sr}_x)_2\text{CoO}_4$ override the crystal anisotropy in oxygen exchange kinetics." *Chem. Mater.*, **27**, 5436 (2015).
20. D. Oh, D. Gostovic, and E. D. Wachsman, "Mechanism of $\text{La}_{0.6}\text{Sr}_{0.4}\text{Co}_{0.2}\text{Fe}_{0.8}\text{O}_3$ cathode degradation." *J. Mater. Res.*, **27**, 1992 (2012).
21. A. K. Opitz et al., "The chemical evolution of the $\text{La}_{0.6}\text{Sr}_{0.4}\text{CoO}_{3-\delta}$ surface under SOFC operating conditions and its implications for electrochemical oxygen exchange activity." *Topics in Catalysis*, **61**, 2129 (2018).
22. F. Pişkin, R. Bliem, and B. Yildiz, "Effect of crystal orientation on the segregation of aliovalent dopants at the surface of $\text{La}_{0.6}\text{Sr}_{0.4}\text{CoO}_{3-\delta}$." *J. Mater. Chem. A*, **6**, 14136 (2018).
23. T. Degen, M. Sadki, E. Bron, U. König, and G. Nénert, "The highscore suite." *Powder Diffraction*, **29**, S13 (2014).
24. G. Holzlechner, M. Kubicek, H. Hutter, and J. Fleig, "A novel ToF-SIMS operation mode for improved accuracy and lateral resolution of oxygen isotope measurements on oxides." *J. Analytical Atomic Spectrometry*, **28**, 1080 (2013).
25. M. Kubicek, G. Holzlechner, A. K. Opitz, S. Larissegger, H. Hutter, and J. Fleig, "A novel ToF-SIMS operation mode for sub 100 nm lateral resolution: application and performance." *Appl. Surf. Sci.*, **289**, 407 (2014).
26. G. M. Rupp, H. Tellez, J. Druce, A. Limbeck, T. Ishihara, J. Kilner, and J. Fleig, "Surface chemistry of $\text{La}_{0.6}\text{Sr}_{0.4}\text{CoO}_{3-\delta}$ thin films and its impact on the oxygen surface exchange resistance." *J. Mater. Chem. A*, **3**, 22759 (2015).
27. S. Tanuma, C. J. Powell, and D. R. Penn, "Calculation of electron inelastic mean free paths (IMFPs) VII. Reliability of the TPP-2M IMFP predictive equation." *Surface and Interface Analysis*, **35**, 268 (2003).
28. J. H. Scofield, *Theoretical Photoionization Cross Sections from 1 to 1500 keV* (California Univ., Lawrence Livermore Lab., Livermore) (1973), Tech. rep..
29. M. Kubicek, G. M. Rupp, S. Huber, A. Penn, A. K. Opitz, J. Bernardi, M. Stoeger-Pollach, H. Hutter, and J. Fleig, "Cation diffusion in $\text{La}_{0.6}\text{Sr}_{0.4}\text{CoO}_{3-\delta}$ below 800 °C and its relevance for Sr segregation." *Phys. Chem. Chem. Phys.*, **16**, 2715 (2014).
30. Z. Cai, M. Kubicek, J. Fleig, and B. Yildiz, "Chemical Heterogeneities on $\text{La}_{0.6}\text{Sr}_{0.4}\text{CoO}_{3-\delta}$ Thin Films Correlations to Cathode Surface Activity and Stability." *Chem. Mater.*, **24**, 1116 (2012).
31. G. M. Rupp, A. Limbeck, M. Kubicek, A. Penn, M. Stöger-Pollach, G. Friedbacher, and J. Fleig, "Correlating surface cation composition and thin film microstructure with the electrochemical performance of lanthanum strontium cobaltite (LSC) electrodes." *J. Mater. Chem. A*, **2**, 7099 (2014).
32. W. Araki, M. Miyashita, and Y. Arai, "Strontium surface segregation in $\text{La}_{0.6}\text{Sr}_{0.4}\text{Co}_{0.2}\text{Fe}_{0.8}\text{O}_{3-\delta}$ subjected to mechanical stress." *Solid State Ionics*, **290**, 18 (2016).
33. Y. Yu, K. F. Ludwig, J. C. Woicik, S. Gopalan, U. B. Pal, T. C. Kaspar, and S. N. Basu, "Effect of Sr content and strain on Sr surface segregation of $\text{La}_{1-x}\text{Sr}_x\text{Co}_{2-y}\text{Fe}_{0.8}\text{O}_{3-\delta}$ as cathode material for solid oxide fuel cells." *ACS Appl. Mater. Interfaces*, **8**, 26704 (2016).
34. D. Tripkovic, J. Wang, R. Küngas, M. B. Mogensen, B. Yildiz, and P. V. Hendriksen, "Thermally controlled activation and passivation of surface chemistry and oxygen-exchange kinetics on a perovskite oxide." *Chem. Mater.*, **34**, 1722 (2022).
35. C. Riedl, M. Siebenhofer, A. Nennung, A. Schmid, M. Weiss, C. Rameshan, A. Limbeck, M. Kubicek, A. K. Opitz, and J. Fleig, "In-situ techniques reveal the true capabilities of SOFC cathode materials and their surface degradation due to omnipresent sulfur trace impurities." *J. Mater. Chem. A*, **11**, 14838 (2022).
36. A. Schmid, A. Nennung, A. Opitz, M. Kubicek, and J. Fleig, "High oxygen exchange activity of pristine $\text{La}_{0.6}\text{Sr}_{0.4}\text{FeO}_{3-\delta}$ films and its degradation." *J. Electrochem. Soc.*, **167**, 124509 (2020).
37. K. Develos-Bagarinao, J. De Vere, H. Kishimoto, T. Ishiyama, K. Yamaji, T. Horita, and H. Yokokawa, "Oxygen surface exchange properties and surface segregation behavior of nanostructured $\text{La}_{0.6}\text{Sr}_{0.4}\text{Co}_{0.2}\text{Fe}_{0.8}\text{O}_{3-\delta}$ thin film cathodes." *Phys. Chem. Chem. Phys.*, **21**, 7183 (2019).
38. M. Kubicek, A. Limbeck, T. Frömling, H. Hutter, and J. Fleig, "Relationship between cation segregation and the electrochemical oxygen reduction kinetics of $\text{La}_{0.6}\text{Sr}_{0.4}\text{CoO}_{3-\delta}$ thin film electrodes." *J. Electrochem. Soc.*, **158**, B727 (2011).
39. E. Bucher, C. Gspan, F. Hofer, and W. Sitte, "Sulphur poisoning of the SOFC cathode material $\text{La}_{0.6}\text{Sr}_{0.4}\text{CoO}_{3-\delta}$." *Solid State Ionics*, **238**, 15 (2013).
40. M. Niania, R. Podor, T. B. Britton, C. Li, S. J. Cooper, N. Svetkov, S. Skinner, and J. Kilner, "In situ study of strontium segregation in $\text{La}_{0.6}\text{Sr}_{0.4}\text{Co}_{0.2}\text{Fe}_{0.8}\text{O}_{3-\delta}$ in ambient atmospheres using high-temperature environmental scanning electron microscopy." *J. Mater. Chem. A*, **6**, 14120 (2018).

41. R. Budiman, S. Liu, K. Bagarinao, T. Ishiyama, H. Kishimoto, K. Yamaji, T. Horita, and H. Yokokawa, "Determination of factors governing surface composition and degradation of $\text{La}_{0.6}\text{Sr}_{0.4}\text{Co}_{0.2}\text{Fe}_{0.8}\text{O}_{3-\delta}$ electrode under sulfur-contained air." *J. Electrochem. Soc.*, **166**, F414 (2019).
42. F. Wang, H. Kishimoto, T. Ishiyama, K. Develos-Bagarinao, K. Yamaji, T. Horita, and H. Yokokawa, "A review of sulfur poisoning of solid oxide fuel cell cathode materials for solid oxide fuel cells." *J. Power Sources*, **478**, 228763 (2020).
43. C. Nicollet, C. Toparli, G. F. Harrington, T. Defferriere, B. Yildiz, and H. L. Tuller, "Acidity of surface-infiltrated binary oxides as a sensitive descriptor of oxygen exchange kinetics in mixed conducting oxides." *Nat. Catal.*, **3**, 913 (2020).
44. E. Mutoro, E. J. Crumlin, M. D. Biegalski, H. M. Christen, and Y. Shao-Horn, "Enhanced oxygen reduction activity on surface-decorated perovskite thin films for solid oxide fuel cells." *Energy Environ. Sci.*, **4**, 3689 (2011).
45. E. J. Crumlin, E. Mutoro, Z. Liu, M. E. Grass, M. D. Biegalski, Y.-L. Lee, D. Morgan, H. M. Christen, H. Blum, and Y. Shao-Horn, "Surface strontium enrichment on highly active perovskites for oxygen electrocatalysis in solid oxide fuel cells." *Energy Environ. Sci.*, **5**, 6081 (2012).
46. M. A. Niania, A. K. Rossall, J. A. Van den Berg, and J. A. Kilner, "The effect of sub-surface strontium depletion on oxygen diffusion in $\text{La}_{0.6}\text{Sr}_{0.4}\text{Co}_{0.2}\text{Fe}_{0.8}\text{O}_{3-\delta}$." *J. Mater. Chem. A*, **8**, 19414 (2020).
47. C. Nicollet and H. L. Tuller, "Perspective on the Relationship between the Acidity of perovskite oxides and their oxygen surface exchange kinetics." *Chem. Mater.*, **34**, 991 (2022).
48. J. Mizusaki, M. Yoshihiro, S. Yamauchi, and K. Fueki, "Nonstoichiometry and defect structure of the perovskite-type oxides $\text{La}_{1-x}\text{Sr}_x\text{FeO}_{3-\delta}$." *J. Solid State Chem.*, **58**, 257 (1985).
49. J. Mizusaki, Y. Mima, S. Yamauchi, K. Fueki, and H. Tagawa, "Nonstoichiometry of the perovskite-type oxides $\text{La}_{1-x}\text{Sr}_x\text{CoO}_{3-\delta}$." *J. Solid State Chem.*, **80**, 102 (1989).
50. D. Tripković, J. Wang, R. Küngas, M. B. Mogensen, B. Yildiz, and P. V. Hendriksen, "Thermally Controlled Activation and Passivation of Surface Chemistry and Oxygen-Exchange Kinetics on a Perovskite Oxide." *Chem. Mater.*, **34**, 1722 (2022).